A wall-layer model for large-eddy simulations of turbulent flows with/out pressure gradient

C. Duprat, G. Balarac, O. Métais, P. M. Congedo, and O. Brugière
LEGI, Grenoble-INP, CNRS—Modélisation et Simulation de la Turbulence (MoST), 1024 rue de la Piscine, 38041 Grenoble, France

(Received 10 November 2010; accepted 23 November 2010; published online 6 January 2011)

In this work, modeling of the near-wall region in turbulent flows is addressed. A new wall-layer model is proposed with the goal to perform high-Reynolds number large-eddy simulations of wall bounded flows in the presence of a streamwise pressure gradient. The model applies both in the viscous sublayer and in the inertial region, without any parameter to switch from one region to the other. An analytical expression for the velocity field as a function of the distance from the wall is derived from the simplified thin-boundary equations and by using a turbulent eddy coefficient with a damping function. This damping function relies on a modified van Driest formula to define the mixing-length taking into account the presence of a streamwise pressure gradient. The model is first validated by *a priori* comparisons with direct numerical simulation data of various flows with and without streamwise pressure gradient and with eventual flow separation. Large-eddy simulations are then performed using the present wall model as wall boundary condition. A plane channel flow and the flow over a periodic arrangement of hills are successively considered. The present model predictions are compared with those obtained using the wall models previously proposed by Spalding, Trans. ASME, J. Appl. Mech **28**, 243 (2008) and Manhart *et al.*, Theor. Comput. Fluid Dyn. **22**, 243 (2008). It is shown that the new wall model allows for a good prediction of the mean velocity profile both with and without streamwise pressure gradient. It is shown than, conversely to the previous models, the present model is able to predict flow separation even when a very coarse grid is used. © *2011 American Institute of Physics*. [doi:10.1063/1.3529358]

I. INTRODUCTION

Because of the development of computational resources, it is current to simulate high Reynolds number flows in complex geometry for practical engineering applications related, for instance, to aeronautical or car industry. To adequately represent the flow unsteadiness, large-eddy simulation (LES) methods are more and more often used. It is well known that the scaling of the near-wall structure is strongly dependent on the Reynolds number, so a very refined grid needs to be used close to the wall if one wants to fully resolved this flow region. An estimation of a LES calculation total cost was provided by Chapman.[1] He showed that the cost of a wall-resolved LES is proportional to $\mathrm{Re}^{2.4}$. The near-wall resolution is thus a strong limit for the LES methods at high Reynolds number. To bypass this limitation, various methods have been proposed. A first approach consists of keeping a fine grid at the wall but solving simplified set of equations weakly coupled to the outer flow. This approach was first employed by Balaras *et al.*,[2] who employed a simplified set of equations, using thin-boundary-layer assumption, in the inner layer. Another example is the detached eddy simulation (DES) method introduced by Spalart *et al.*,[3] which switches from one turbulence model in the core of the flow to another one in the wall vicinity. A lot of works has more recently been devoted to the development of the so-called hybrid methods, using RANS equations in the inner layer, while LES equations are solved away from the wall (see Fröhlich and von Terzi,[4] for a recent review). Another approach consists in using a relatively coarse grid at the wall and to mimic the dynamical effects of the energy-containing eddies in the wall-layer through a wall model. The model allows then to specify proper wall boundary conditions by enforcing the wall shear-stresses value. Such models were first employed by Schumann[5] in a channel flow simulation. Modification of Shumann's model has been proposed later by Grötzbach[6] and Spalding,[7] for example. A review of wall model used in LES can be found in various references.[8–10] Note that previous wall stress models made the assumption of an equilibrium boundary-layer, which is not valid in many complex flows, in particular, flows with boundary-layer separation. The favorable or adverse pressure gradient indeed acts as a nonequilibrium term for the boundary-layer. To take this effect into account, Manhart *et al.*[11] proposed a model including the streamwise pressure gradient. However, the Reynolds stresses were neglected in their formulation limiting the validity range of the model to the viscous sublayer.

The purpose of the present work is to extend the work of Manhart *et al.*[11] with a new model for the streamwise velocity taking into account both the streamwise pressure gradient and the Reynolds stresses effects. This new model provides an analytical formulation of the streamwise velocity variation as a function of the distance to the wall. After the presentation of the model formalism (Sec. II), it is first validated *a priori* by comparison with direct numerical simulation (DNS) data (Sec. III). Using a so-called *a posteriori* approach, the model has then been implemented to perform LES of various boundary-layer flows (Sec. IV). The considered boundary-layer flows consist in a periodic channel and a periodic arrangement of hills. The results are compared with the wall-resolved LES of Kravchenko *et al.*[12] for the channel flow and the wall-resolved LES of Temmerman *et al.*[13] and Breuer *et al.*[14] for the periodic hill configuration. The model performances are evaluated by comparing its predictions with those obtained with the previous models, respectively, proposed by Spalding[7] and Manhart *et al.*[11] It is shown that the strength of the present wall model lies in its ability to predict flow separation and reattachement even with a coarse grid.

II. GOVERNING EQUATION AND WALL MODELING STRATEGY

One of the starting point for a wall model is to consider averaged Navier–Stokes equations. In the LES case, it consists in assuming that the filtered velocity is equivalent to the averaged velocity close to the wall. Piomelli[10] showed that this assumption can be done if cells are coarse enough close to the wall to contain a large number of eddies and if the time step is much larger than the time-scale characteristic of the near-wall eddies. In the boundary-layer case, a simplified averaged set of partial equations derived from the Navier–Stokes equations can be considered. This set of equations, known as the unsteady thin-boundary-layer equations[8] (TBLE), is

$$\frac{\partial U_i}{\partial t} + \frac{\partial (U_i U_j)}{\partial x_j} + \frac{1}{\rho}\frac{\partial P}{\partial x_i} = \frac{\partial}{\partial y}\left[(\nu+\nu_t)\frac{\partial U_i}{\partial y}\right]. \quad (1)$$

In this equation, ν and ρ are, respectively, the fluid kinematic viscosity and the density, assumed to be constant. U_i is the mean velocity in directions x_i and y indicates the direction normal to the wall. The Reynolds stresses are modeled through a turbulent eddy viscosity assumption noted $\nu_t(\vec{x},t)$. The left-hand side of the previous equation corresponds to the nonequilibrium terms. Starting from Eq. (1), Wang and Moin[15] compared two simpler models to a full TBLE model: first, totally neglecting the left-hand side and second including only the streamwise pressure gradient. They showed that the inclusion of the pressure gradient allows for a significant improvement of the model predictions. In the present work, we thus reduce the left-hand side of the equation to the pressure gradient term. The streamwise pressure gradient is furthermore assumed to be constant in the wall-normal direction. Under these assumptions, the simplified mean streamwise momentum equation can be integrated analytically in the wall normal direction,

$$0 = (\nu+\nu_t)\frac{\partial U}{\partial y} - \frac{1}{\rho}\frac{\partial P}{\partial x}y - \frac{\tau_w}{\rho}, \quad (2)$$

leading to

$$\frac{\partial U}{\partial y} = \frac{\frac{\partial P}{\partial x}y + \tau_w}{\rho(\nu+\nu_t)}, \quad (3)$$

with U the mean streamwise velocity and τ_w the wall-shear stress defined as $\tau_w = \rho\nu \frac{\partial U}{\partial y}\big|_{y=0}$.

A. Near-wall scaling of Manhart *et al.*

Next, momentum equation Eq. (3) is scaled with the extended inner scaling proposed by Manhart *et al.*[11] for the wall-layer. This scaling is denoted by a superscript *. Actually, the scaling takes into account both the wall shear stress and the streamwise pressure gradient. Nondimensional velocity U^* and nondimensional length y^* are thus defined by

$$U^* = \frac{U}{u_{\tau p}}, \quad y^* = \frac{y u_{\tau p}}{\nu}, \quad (4)$$

where $u_{\tau p} = \sqrt{u_\tau^2 + u_p^2}$ is a combined velocity using the classical friction velocity at the wall, $u_\tau = \sqrt{|\tau_w|/\rho}$, and an additional velocity based on the streamwise pressure gradient $u_p = |(\mu/\rho^2)(\partial P/\partial x)|^{1/3}$ proposed by Simpson.[16] One of the advantages of this scaling is that it stays valid even for separation or reattachment region as opposed to the classical wall coordinates (where $u_\tau = 0$). Moreover, a nondimensional parameter $\alpha = u_\tau^2/u_{\tau p}^2 \in [0,1]$ can be used to quantify the preponderant effect between shear stress and streamwise pressure gradient. Hence, $\alpha = 0$ corresponds to a zero shear stress flow, a separation point, and $\alpha = 1$ corresponds to a zero pressure gradient flow.

From dimensional equation (3), the following nondimensional formula can be derived using the extended scaling:

$$\frac{\partial U^*}{\partial y^*} = \frac{\mathrm{sign}\left(\frac{\partial P}{\partial x}\right)(1-\alpha)^{3/2} y^* + \mathrm{sign}(\tau_w)\alpha}{\left(1 + \frac{\nu_t}{\nu}\right)}. \quad (5)$$

The comparison between the pressure gradient sign and the wall shear stress sign allows to know if the pressure gradient is adverse or favorable.

B. Turbulent eddy viscosity model

Now, the eddy viscosity ν_t needs to be defined. It is usually modeled using an *ad hoc* damped mixing-length to approximate both the linear and the inertial region. Even if the original van Driest formula[17] predicts very well the velocity profile for boundary-layers with zero streamwise pressure gradient, it has given unsatisfactory results for nonzero pressure gradient. This has prompted many investigators[18,19] to propose modifications for this turbulent viscosity to take the pressure gradient into account. Based on the works of Nituch *et al.*[20] and Balaras *et al.*,[2] the eddy viscosity is here defined by

$$\frac{\nu_t}{\nu} = \kappa y^*[\alpha + y^*(1-\alpha)^{3/2}]^\beta (1 - e^{-y^*/(1+A\alpha^3)})^2, \quad (6)$$

where κ is the von Kàrmàn constant. The constants A and β are determined through *a priori* results as discussed in Sec. III.

The last two equations, (5) and (6), allow to relate the streamwise velocity with the wall-normal coordinate, taking into account both streamwise pressure gradient and velocity gradient at the wall. They constitute the present wall model allowing to determine the wall shear stress, which is the needed unknown quantity in practical LES.

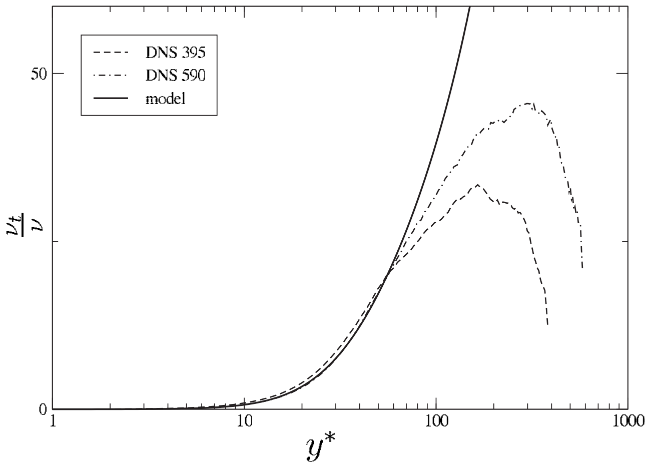

FIG. 1. Comparison of ν_t/ν for $\alpha=1$, DNS channel flow.

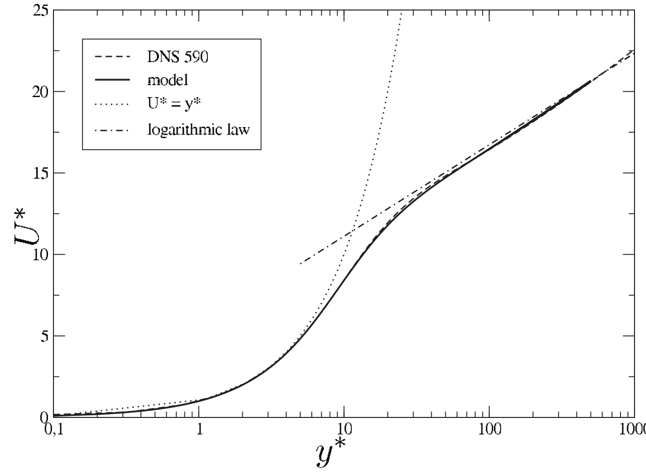

FIG. 3. Comparison of the mean nondimensional velocity profile $\alpha=1$.

III. *A PRIORI* VALIDATION

A. Asymptotic behavior

To validate the model for U^*, two asymptotic cases are first considered. First, in the viscous sublayer, y^* is very small and the turbulent viscosity can be assumed to be zero. Equation (5) can be integrated in the wall-normal direction y^*, to get a polynomial expression for the velocity profile,

$$U^* = \mathrm{sign}\left(\frac{\partial P}{\partial x}\right)\frac{(1-\alpha)^{3/2}}{2}y^{*2} + \mathrm{sign}(\tau_w)\alpha y^*. \quad (7)$$

The model proposed by Manhart *et al.*[11] is thus recovered with the streamwise pressure introducing a quadratic term, neglected in the classical linear wall law. A second asymptotic case consists in considering the inertial region with zero streamwise pressure gradient. In this case, the damping function of the turbulent viscosity is close to one and $\alpha=1$. The streamwise velocity then follows the classical logarithmic law,

$$U^* = \frac{\mathrm{sign}(\tau_w)}{\kappa}\ln(y^*) + C^{ste}. \quad (8)$$

B. Comparison with DNS data

To check the validity range of the present model described by Eqs. (5) and (6), *a priori* tests based on DNS calculations for different flow configurations are next presented. DNS results are used to validate both turbulent viscosity and velocity models in the extended coordinate system. Three different configurations are used: a simple periodic channel flow at different Reynolds numbers ($Re_\tau=395$ and 590) (CF), a separating turbulent boundary-layer along a flat plate (BL), and a channel flow with constrictions (PH). Channel flow calculations were performed by Moser *et al.*[21] and the last two DNSs were done by Manhart *et al.*[11] All DNS calculations are periodic in the spanwise direction so the average fields depend only on the streamwise and wall normal directions. This allows to calculate α at the wall at each streamwise position. The value of α is then used to classify the configuration.

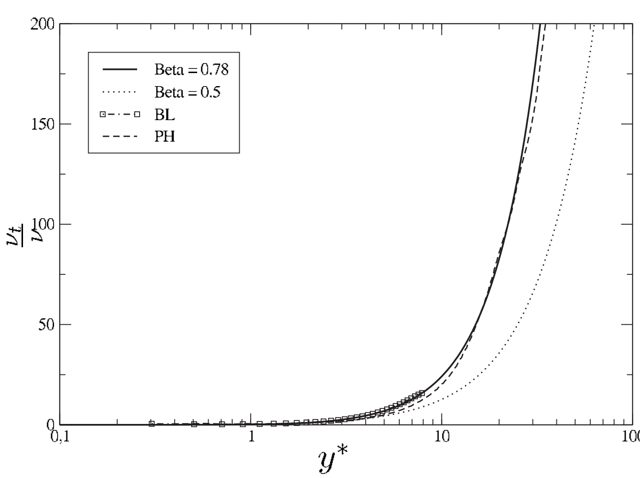

FIG. 2. Comparison of ν_t/ν for $\alpha=0$, separation point.

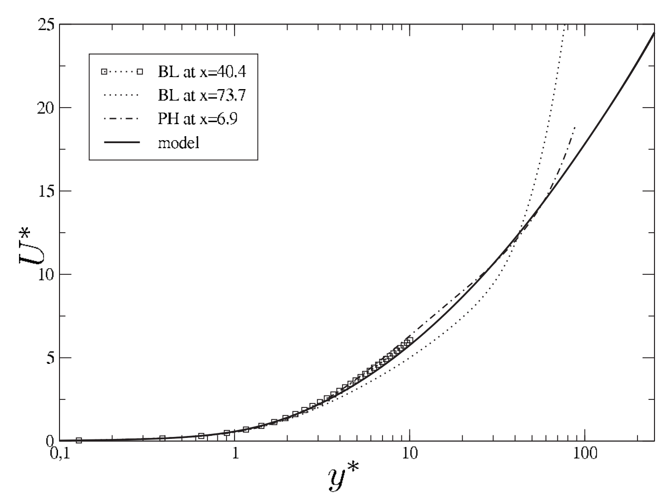

FIG. 4. Comparison of the mean nondimensional velocity profile for $\alpha=0.3$ and $\mathrm{sign}(\tau_w)\cdot\mathrm{sign}(\partial P/\partial x)>0$.

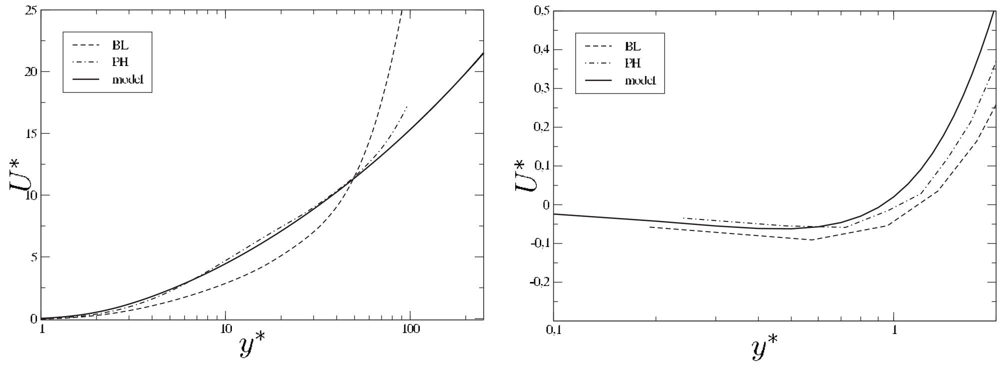

FIG. 5. Comparison of the mean nondimensional velocity profile for $\alpha=0.3$ and $\text{sign}(\tau_w)\cdot\text{sign}(\partial P/\partial x)<0$.

1. Turbulent viscosity

Figure 1 shows the turbulent viscosity extracted from DNS data through the relation $\nu_t=-\langle u'v'\rangle/(\partial U/\partial y)$ in the $\alpha=1$ case (CF) corresponding to a zero pressure gradient flow. Here u' and v' are the velocity fluctuations in the streamwise and wall-normal directions and the brackets are the averaging operator both in time and along the homogenous directions. The computed turbulent viscosity is compared with the model given by Eq. (6). A good agreement between the model and the DNS data is found for distance from the wall as far as $y^*\approx 60$. This indicates that the model for the turbulent viscosity is correct in the absence of streamwise pressure gradient. We next consider the cases where separation occurs and Fig. 2 shows the turbulent viscosity profile at the separation point ($\alpha=0$). From these DNS data, the best choice for β is found to be $\beta=0.78$ which is higher than the previously chosen value[20] of $\beta=0.5$. Moreover, Figs. 1 and 2 allow to validate the damping function given by $(1-e^{-y^*/(1+A\alpha^3)})$: the best fit is obtained for $A=17$. Note that for a value of $\alpha=1$, i.e., without pressure gradient, this gives a damping function equal to $(1-e^{-y^*/18})$ which is very close to the damping functions used by Wang and Moin[15] and by Cabot and Moin:[8] $(1-e^{-y^*/19})$ and $(1-e^{-y^*/17})$, respectively. It is interesting to note that the damping function depends on the value of α, that is to say on the intensity of the pressure gradient, as it was suggested in previous studies.[18]

2. Mean velocity profile

Figures 3–5 show the mean velocity profiles in the extended scaling for different values of α. Knowing the value of α, the nondimensional velocity U^* can then be computed as a function of the nondimensional distance from the wall y^*, from Eqs. (5) and (6). These profiles are superposed with the DNS data on the figures. The classical attached flow with zero pressure gradient is first represented on Fig. 3. It is well known that the law of the wall has a linear part in the viscous region and the classical logarithmic profile in the inertial region. A very close agreement between the model and the velocity profile from the channel DNS calculation is observed. In particular, the buffer layer is well predicted.

We next consider the pressure gradient dominated situation, $\alpha=0.3$. It is necessary to distinguish between two cases depending on the pressure gradient sign in comparison with the wall shear stress signs. Figures 4 and 5 show, respectively, the favorable and adverse pressure gradient cases. In both cases, our extended wall model approximates the profiles correctly. In particular, the reverse flow existing close to the wall after the separation point $[\text{sign}(\tau_w)\cdot\text{sign}(\partial P/\partial x)<0]$ is well predicted (see zoom on Fig. 5, left). Finally, when the wall shear stress is zero, corresponding to a separation point ($\alpha=0$), the model predicts the velocity correctly for all DNS data cases (see Fig. 6).

IV. *A POSTERIORI* TESTS

In this section, LESs are performed using various wall models as wall boundary condition. To test the performance of the present model given by Eqs. (5) and (6), it is compared with two previous wall models: the model proposed by Spalding[7] (denoted as SWM) and the one by Manhart *et al.*[11] (denoted as MPB). The choice of these two models is motivated by the fact that SWM model assumes zero longitudinal pressure gradient and that MPB model, although taking into account longitudinal pressure gradients, is only valid if the first computational point is located in the viscous layer.

Spalding's wall model (noted SWM) uses a Taylor series expansion to describe, with a unique function, the entire turbulent boundary-layer: viscous region, buffer layer, and logarithmic region. Using the classical wall units,

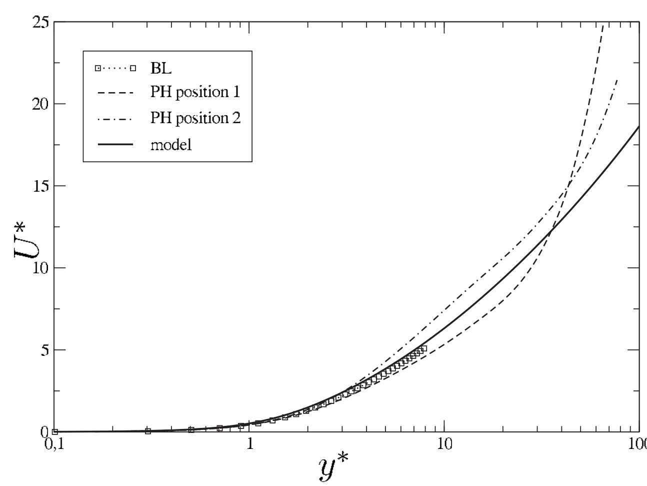

FIG. 6. Comparison of the mean nondimensional velocity profile at the separation point $\alpha=0$.

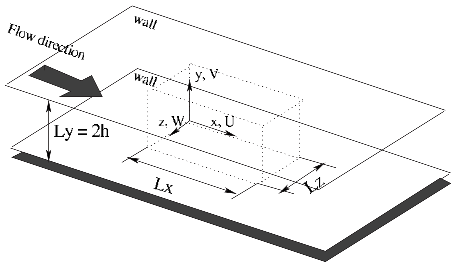

FIG. 7. Sketch of the channel flow test case.

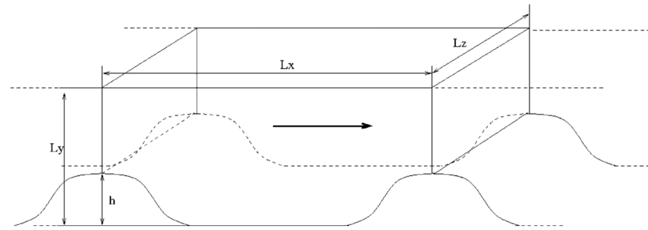

FIG. 8. Sketch of the periodic hill flow test case.

$$U^+ = \frac{U}{u_\tau}, \quad y^+ = \frac{yu_\tau}{\nu}, \tag{9}$$

Spalding's law writes as

$$y^+ = U^+ + \frac{1}{E}\left\{ e^{-\kappa U^+} - \left[1 + (\kappa U^+) + \frac{(\kappa U^+)^2}{2} + \frac{(\kappa U^+)^3}{6} \right] \right\}, \tag{10}$$

where $\kappa = 0.42$ is the von Kàrmàn constant and E a constant characterizing the wall roughness: $E = 9.1$ for a smooth wall. Note that this wall function is only valid for flows with zero pressure gradient such as the classical channel flow. As previously pointed out (see Sec. III A), Manhart *et al.*[11] is identical to our model when the Reynolds stresses are neglected in front of the viscous stress. It is thus restricted to computations with a first computational point away from the wall located within the viscous sublayer. This model is given, Eq. (7), and referred to as the MPB model. Note that this wall model has only been validated through *priori* tests by Manhart *et al.*[11]

A. Numerical methods and subgrid-scale model

The governing equations are solved using the open source CFD code, OPENFOAM. It uses finite volume methods and has been extensively validated for LES.[22–24] The spatial discretization scheme is second-order accurate and uses centered interpolations and differentiations. The temporal scheme is a second-order accurate Crank–Nicholson scheme. The Rhie and Chow momentum interpolation[25] is applied to avoid pressure-velocity decoupling. The Poisson equation for the pressure increment is solved iteratively using incomplete Cholesky conjugate gradient methods. Parallelization is implemented via domain decomposition.

The application of the spatial filtering operation to the incompressible Navier–Stokes equations leads to the following filtered equations:

$$\frac{\partial \bar{u}_i}{\partial t} + \frac{\partial \bar{u}_i \bar{u}_j}{\partial x_j} = -\frac{1}{\rho}\frac{\partial \bar{p}}{\partial x_i} + \frac{\partial}{\partial x_j}\left(\nu \frac{\partial \bar{u}_i}{\partial x_j} - \tau_{ij} \right), \tag{11}$$

where $\tau_{ij} = \overline{u_i u_j} - \bar{u}_i \bar{u}_j$ represents the unknown subgrid-scale stresses, which has to be modeled in LES. In this study, the subgrid-scale (SGS) model is based on the eddy-viscosity concept, leading to

$$\tau_{ij} - \tfrac{1}{3}\delta_{ij}\tau_{kk} = -2\nu_{\text{SGS}}\bar{S}_{ij}, \tag{12}$$

where $\bar{S}_{ij} = 1/2(\partial \bar{u}_i/\partial x_j + \partial \bar{u}_j/\partial x_i)$ and ν_{SGS} is the subgrid-scale (SGS) viscosity. The contribution τ_{kk} is lumped into a modified pressure, $\bar{P} = \bar{p} - \frac{1}{3}\tau_{kk}$, and therefore does not need to be accounted for. Using the SGS viscosity, the filtered equations lead to the LES equations,

$$\frac{\partial \bar{u}_i}{\partial t} + \frac{\partial \bar{u}_i \bar{u}_j}{\partial x_j} = -\frac{1}{\rho}\frac{\partial \bar{P}}{\partial x_i} + \frac{\partial}{\partial x_j}\left[(\nu + \nu_{\text{SGS}})\frac{\partial \bar{u}_i}{\partial x_j} \right]. \tag{13}$$

The SGS model we used is the model of Yoshizawa and Horiuti[26] based on a transport equation for the subgrid kinetic energy, $k_{\text{SGS}} = 1/2\tau_{kk}$. This model was here chosen because models with transport equation have shown to yield better results when very loose grid are used.[22] Once k_{SGS} is determined, the SGS viscosity is subsequently derived as

$$\nu_{\text{SGS}} = C_k \Delta \sqrt{k_{\text{SGS}}}, \tag{14}$$

where $\Delta = (\Delta x \Delta y \Delta z)^{1/3}$ is a characteristic length scale, taken proportional to an averaged grid size. In most of this work, C_k is taken constant with $C_k = 0.07$ as recommended by Yoshizawa and Horiuti.[26] To check the influence of the subgrid-scale model, some LES computations are performed with a variable C_k determined with the dynamic procedure proposed by Ghosal *et al.*[27] Note that the SGS model implementation in OPENFOAM has already been extensively validated by Fureby *et al.*[22]

In a finite volume solver, Eq. (13) is rewritten as

$$\frac{\partial}{\partial t}\left(\int\int\int_V \bar{u}_i dV \right) + \int\int_{S_j} \bar{u}_i \bar{u}_j dS_j$$
$$= -\frac{1}{\rho}\int\int\int_V \frac{\partial \bar{P}}{\partial x_i} dV + \int\int_{S_j} (\nu + \nu_{\text{SGS}})\frac{\partial \bar{u}_i}{\partial x_j} dS_j, \tag{15}$$

where V is the volume of the cell and S_j is the surface of the cell normal to the direction j. The wall model is then used to define the boundary condition at the wall for the molecular and turbulent viscosity term $(\nu + \nu_{\text{SGS}})\partial \bar{u}_i/\partial y$. For the cells in contact with the wall, this term is rewritten to enforce the wall normal velocity gradient to correspond to the shear stress value given by the wall model. This is performed by using a corrective parameter ν_{corr}, homogeneous to a viscosity, such that

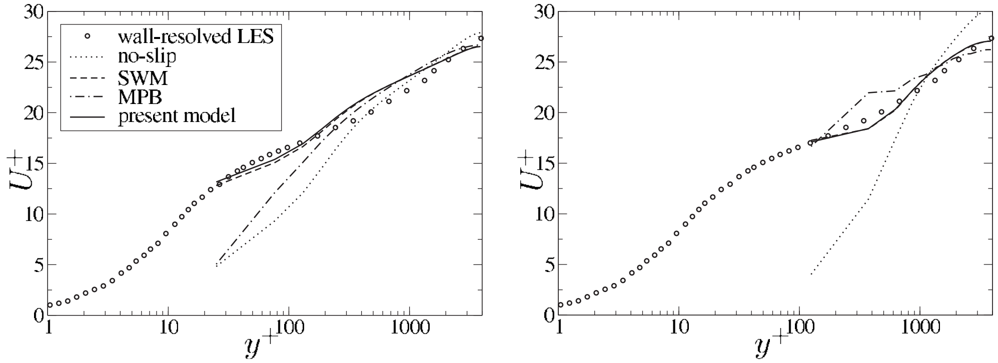

FIG. 9. Profiles of the mean streamwise velocity in wall units for the 64^3 mesh (left) and the 32^3 mesh (right).

$$(\nu+\nu_{\mathrm{SGS}})\frac{\partial \bar{u}_j}{\partial y}=(\nu+\nu_{\mathrm{SGS}}+\nu_{\mathrm{corr}})\left(\frac{\partial \bar{u}_j}{\partial y}\right)^{\oplus}_{\mathrm{wall}}, \tag{16}$$

where $(\partial \bar{u}_j/\partial y)^{\oplus}_{\mathrm{wall}}$ is the velocity gradient computed by the code. To provide the correct velocity derivative in the first cell at the wall, ν_{corr} is thus given by:

$$\nu_{\mathrm{corr}}=\frac{\tau_w}{\rho\left(\dfrac{\partial \bar{u}_j}{\partial y}\right)^{\oplus}_{\mathrm{wall}}}\left(1+\frac{\nu_{\mathrm{SGS}}}{\nu}\right)-\nu-\nu_{\mathrm{SGS}}, \tag{17}$$

where τ_w is determined locally by the wall model using the filtered velocity as a local averaged velocity close to the wall.

B. Simulated flow geometries

We first consider the classical turbulent channel flow which has been extensively used as a simple test case for wall models without streamwise pressure gradient effects. Wall-resolved LES of Kravchenko *et al.*[12] are here used as reference. Similarly to these LESs, simulations are thus performed at $\mathrm{Re}_\tau=4000$, Reynolds number based on the channel half-width h, the friction velocity u_τ, and the kinematic viscosity ν. The size of the computational domain is the same as for the TBLE simulations of Cabot and Moin,[8] $L_x=2\pi h$, $L_y=2h$, and $L_z=2\pi/3h$ in the streamwise x, wall-normal y, and spanwise z, directions, respectively (see Fig. 7). The objectives of the present model are to be used in complex flow geometries at high Reynolds number, that is to say with a loose grid. Similarly to Cabot and Moin,[8] the grid spacing is

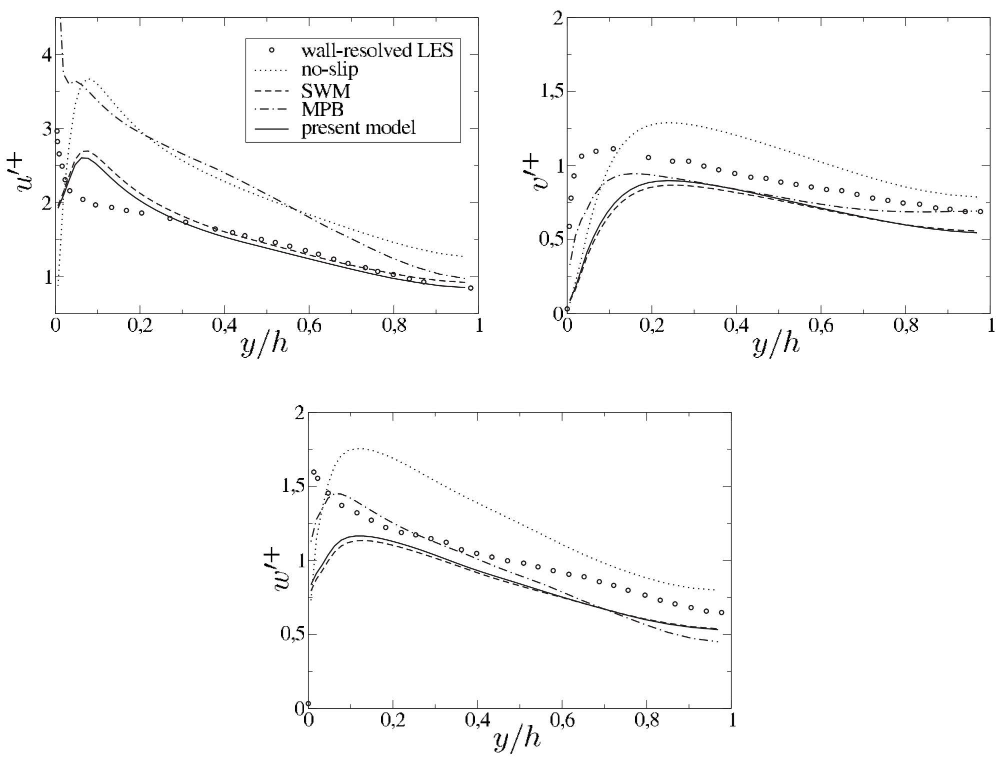

FIG. 10. Profiles of the streamwise (top-left), normal (top-right) and spanwise (bottom) velocity component rms for the 64^3 mesh.

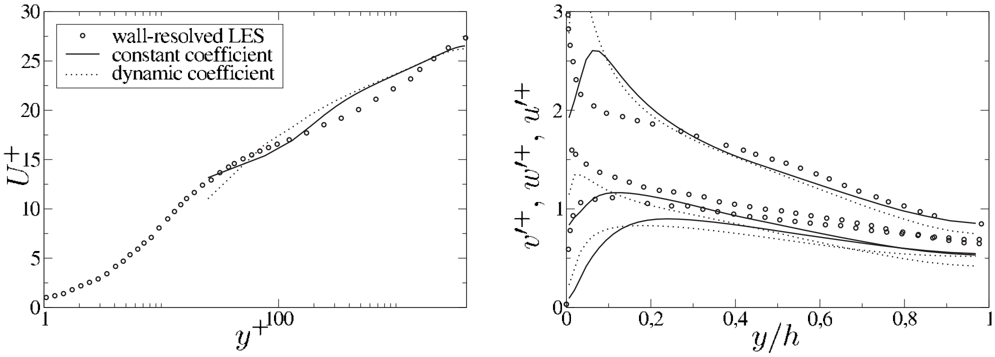

FIG. 11. Profiles of the mean streamwise velocity (left) and the velocity components rms (right) for the 64^3 mesh. Comparison between constant and dynamic C_k used in the SGS model, Eq. (14).

thus taken uniform in each direction (without any wall-refinement), and two different discretizations are thus used which are rather loose by current standard for the channel flow. The first grid consists in 64^3 computational cells with a first grid point located in the buffer layer at 25 wall units away from the wall corresponding with $y_f^+=25$. The second grid is even coarser and composed of 32^3 computational cells with a first grid point in the inertial region such as $y_f^+=120$. It is probably representative of resolutions used in high Reynolds numbers, complex flow configurations. The statistical quantities are obtained by averaging through homogeneous directions (spanwise and streamwise) and by averaging in time over 160 crossing times of the computational domain.

The second simulated flow is the flow over a periodic arrangement of hills (see Fig. 8). It is a challenging flow for wall models since it exhibits a boundary-layer with streamwise pressure gradient due to the streamwise curvature, leading to separation and reattachment processes with a large backflow region. The proper representation of the flow separation constitutes a particularly demanding test. This test case is part of the ERCOFTAC Database collection and was already part of the ERCOFTAC/IAHR/COST Workshop on Refined Turbulence Modeling.[28] A detailed investigation of this flow was undertaken by Fröhlich *et al.*[29] based on LES computation. In conformity with this test case, the dimensions of the geometry are $L_x=9h$, $L_y=3.035h$, and $L_z=4.5h$ (h hill height) as recommended by Mellen *et al.*[30] for LES or hybrid LES-RANS simulations. The Reynolds number based on h, the bulk velocity U_b, and the viscosity ν is fixed to 10 595. In the streamwise (denoted by x) and spanwise (denoted by z) directions, periodic boundary conditions are used. Wall models are applied on the hill surface as well as on the top-wall of the channel. For a given streamwise position x, 33 discretization points are used in the y direction (denoted by vertical direction) and these points are distributed with a constant expansion ratio between two adjacent cells. Three grids (noted A, B, and C) with different expansion rates are chosen such that the distance y_f^+ (expressed in standard wall units) of the first computational point away from the hill wall is $y_f^+=5$ for grid A, $y_f^+=40$ for grid B, and $y_f^+=100$ for grid C. Note that the total number of computational points is therefore identical for the three grids with $n_x=118$, $n_y=33$, and $n_z=96$ in the streamwise, vertical, and spanwise directions, respectively. To obtain reliable statistics, the quantities are averaged in time over 140 crossing times of the computational domain, in conformity with the literature recommendations, and along the spanwise direction. The results are compared with the wall-resolved LES performed by Temmerman *et al.*[13] (TL) and Breuer *et al.*[14] (BM). These wall-resolved LESs were performed with $196\times128\times186$ grid points and $280\times220\times200$ grid points, respectively, using a y_f^+ around 1. It is important to point out that our computational grid has 12.5 times and 33 times less points than the two wall-resolved LES performed by Temmerman *et al.*[13] and Breuer *et al.*,[14] respectively.

C. Results and discussions

1. Channel flow

The channel flow LESs are performed using the three different wall models: the present model, Eqs. (5) and (6), SWM model,[7] and MPB model.[11] In addition, results of the computations without any wall model are also shown for comparison: these are called no-slip boundary conditions. Results are compared with the wall-resolved LES computation by Kravchenko *et al.*,[12] as already done by Cabot and Moin[8] to validate their TBLE simulations.

We first focus on the mean velocity profile and compare the behavior of the various wall models for the two grid resolutions 64^3 ($y_f^+=25$) and 32^3 ($y_f^+=120$). The results are displayed on Fig. 9 and are expressed in wall units taking u_τ from the wall-resolved LES to scale all the data. As expected, the use of a wall model is obviously compulsory: the results obtained for both resolutions without any model (no-slip case) indicate a flow relaminarization due to an underestimation of the wall-shear stress. Similarly, the MPB model is not in its validity region because Reynolds stress tensor terms are not negligible. This leads to an underestimation of the velocity close to the wall for the 64^3 resolution and a bad prediction of the slope in the inertial range. The SWM model and the present model lead to very similar results since, as previously pointed out, both models are designed to match both the linear profile close to the wall and the logarithmic law away from the wall. Even with a very coarse resolution,

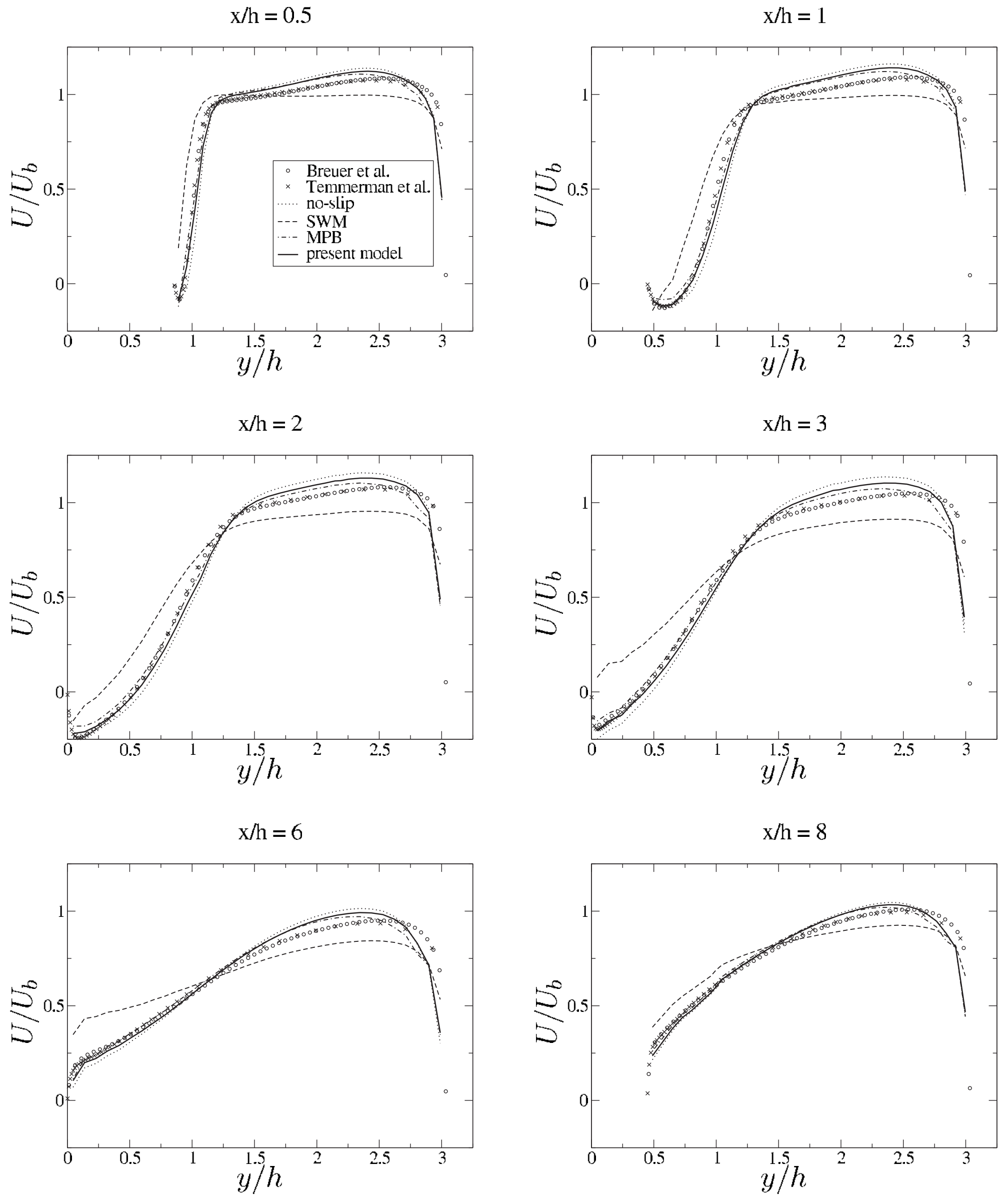

FIG. 12. Profiles of the average streamwise velocity for grid A at different streamwise locations, x/h.

both model predictions are closed to the well-resolved LES results showing their ability to correctly predict the mean velocity within the flow core.

For further analysis, the second-order statistics are shown in Fig. 10. It is important to point out that the wall models used in the present study are not built to properly predict the rms velocity components in the vicinity of the wall since no specific treatment is applied in this region such as a dynamic stochastic forcing proposed by Keating and Piomelli[31] or the synthesized turbulence method proposed by Davidson and Billson.[32] However, one can expect to obtain a correct prediction of these statistical quantities in the channel core. Figure 10 shows that if no-wall model is used, the rms values are ill-predicted throughout the channel depth. For the so-called no-slip boundary condition case, the three rms components are indeed underestimated close to the wall before undergoing a strong increase away from the wall. This too strong increase can be explained by the overestimated mean normal velocity gradient near the wall, which leads to an overestimation of the turbulent production intensity. The turbulent fluctuations are consequently overpredicted over the whole channel width. Similarly, the MPB model strongly overestimates the streamwise fluctuations. For this model, a linear profile, $u^+=y^+$, is assumed in the case without pressure gradient to be valid until the first computational point away from the wall. When this point is not located in the viscous region, the model yields a strong overestimation of the mean normal velocity gradient close to the wall. Both the SWM model and the present model fail to predict the rms statistics close to the wall. For $y/h>0.2$, both models lead, however, to a good prediction of the rms quantities in concordance with the wall-resolved LES. Note that the normal (v') and spanwise (w') velocity fluctuations statistics are weakly un-

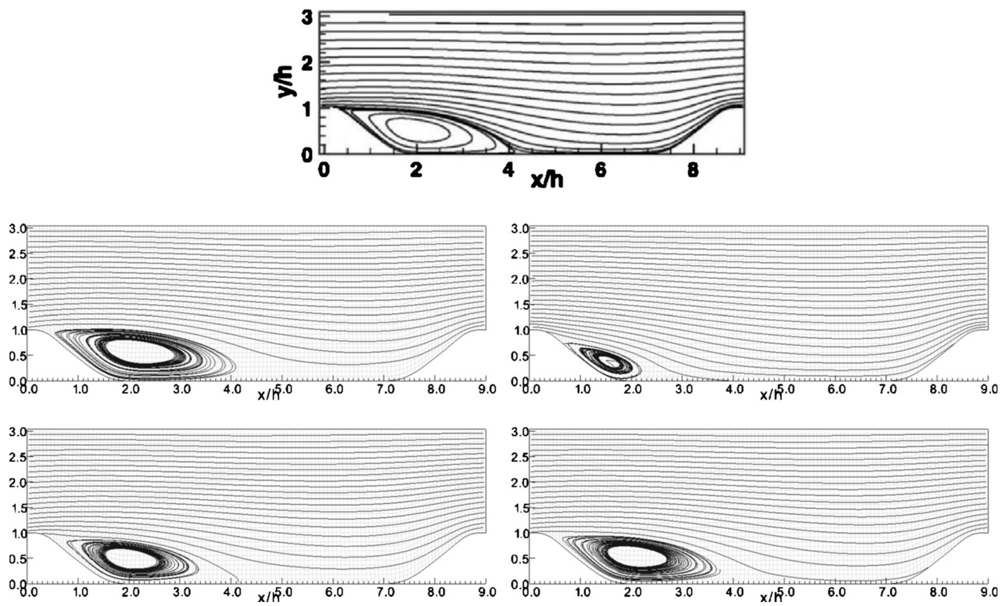

FIG. 13. Mean streamlines for grid A. Top: reference LES computation by Breuer *et al.* (Ref. 14); top to bottom and left to right: no-slip condition, SWM model, MPB model, present model.

derestimated. These results are consistent with the previous observations made by Cabot and Moin[8] based on TBLE computations and by Keating and Piomelli[31] based on DES computations.

To investigate the influence of the sugbgrid-scale model, in particular, in the near-wall region, LESs using the present wall-model are performed with a dynamic determination of C_k for the SGS model given by Ghosal *et al.*[27] (Fig. 11). The mean velocity profiles are similar with both SGS models but some important differences can, however, be noticed for the rms quantities. Indeed, close to the wall, the dynamic procedure predicts a higher level of fluctuation for the three rms components, especially for the u' component. This is due to the well-known fact that the dynamic procedure allows to more correctly reproduce the decay of ν_{SGS} when one approaches the wall and therefore induces a less important damping of the fluctuations in this flow region.[33]

2. Periodic hills

We now consider the periodic hill configuration. As pointed out, the challenge for the wall-models lays in their ability to allow the prediction of flow separation. The correct estimation of the length of the recirculation bubble also constitutes a good quality test for the models. We recall that three different grids are used differing by their near-wall resolution: grid A with $y_f^+=5$, grid B with $y_f^+=40$, and grid C with $y_f^+=100$.

Figure 12 shows the mean velocity profiles obtained with a grid A LES using the different wall models: SWM, present, and MPB models. As for the channel flow, a LES computation without any wall model is also shown. The profiles are displayed at different streamwise locations, x/h, where h is the hill height. For grid A, the first cell point is located at the upper end of the viscous region. The meshing is thus fine enough to lead to good results for the no-model case (no-slip condition). Moreover, MPB model is expected to be within its validity range. Thus, a good agreement with the wall-resolved LES data is found for the MPB and present models over the entire height of the computational domain. Conversely, the SWM model leads to a poor prediction of the mean velocity not only in the vicinity of the hill surface but also in the core of the flow. It is interesting to notice that the no-model case (no-slip) matches much better the reference data than the SWM model. This clearly demonstrates the importance of designing models taking properly into account the effects on the mean quantities of the streamwise pressure gradient. Conversely, the present model and the MPB model allow for slightly better predictions than the no-model case.

This is confirmed by Fig. 13 which shows the mean flow streamlines for the various cases. The results obtained in the reference well-resolved LES by Breuer *et al.*[14] are also displayed for comparison. The size of the separation region size for the SWM model is clearly underestimated, whereas the other wall boundary conditions yield a good agreement with the reference result.

The improved performances of the present model are made more obvious when coarser grid resolutions are used. Figure 14 shows the mean velocity profile at various streamwise locations for the grid C case. As expected, SWM model still leads to poor predictions and is not longer able to predict flow separation as shown by the mean velocity which remains always positive. Similarly, the no-model case is no longer justified and similar results to the SWM model without reverse flow are found. Since the first computational cell is located in the inertial region where Reynolds stresses are important, MPB model fails also to correctly predict the flow close to the wall and no reverse flow is found. Even if its applicability is questionable with grid C wall resolution, one can notice that MPB model provides better results than SWM model especially in the downslope part of the hill ($x/h=1$, $x/h=2$, and $x/h=3$). Only the present model is able to predict the reverse flow with acceptable agreement with

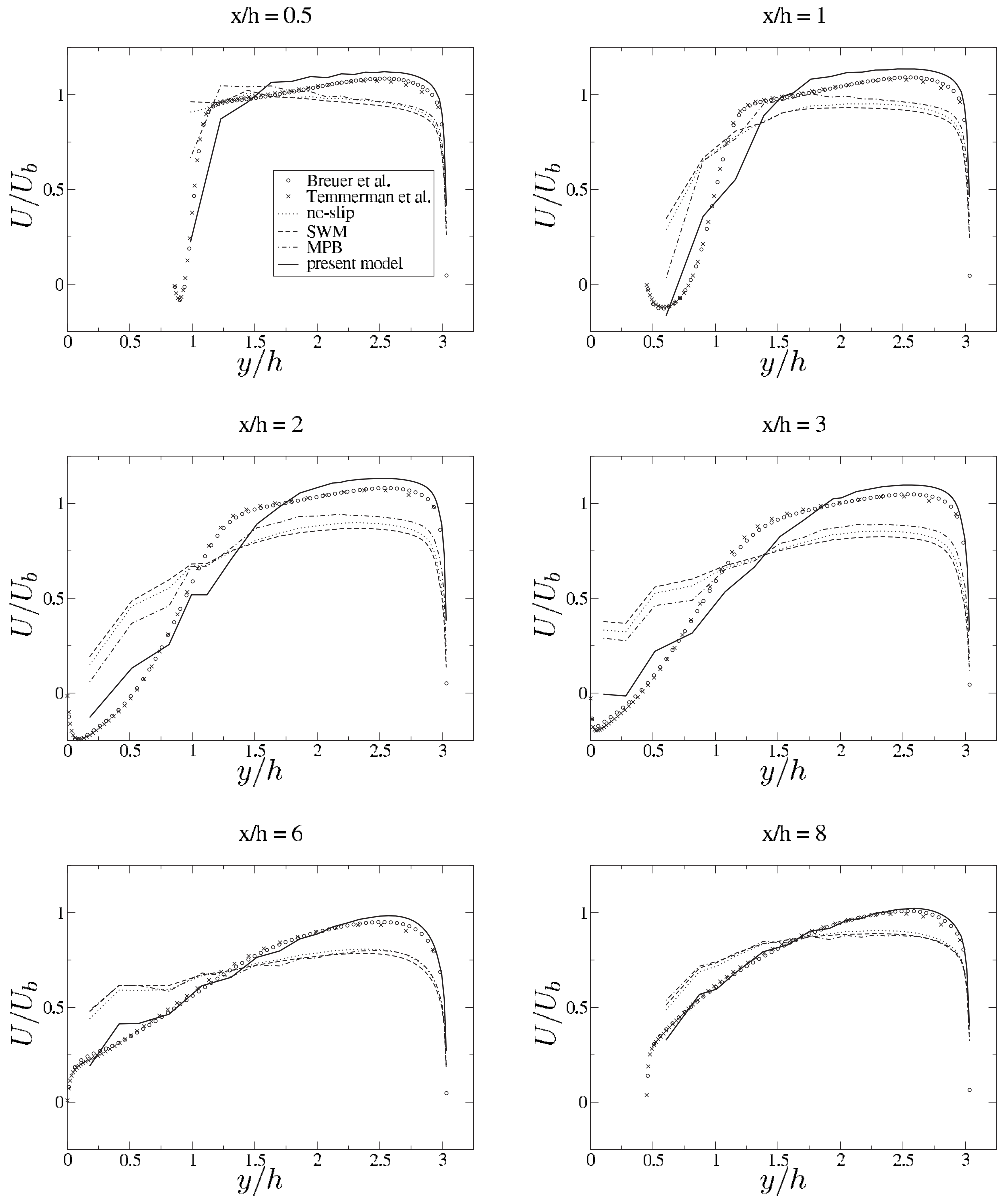

FIG. 14. Profiles of the average streamwise velocity for grid C at different streamwise locations, x/h.

the reference data. The consequence is that, due to mass conservation, only the present model is also able to match the reference data in the core of the flow.

Similar results are found with grid B resolution which has its first cells in the buffer layer. In this case, the MPB model is able to predict a reverse flow but the size of the recirculation is strongly underestimated as shown by Fig. 15. In comparison, the present model allows to reproduce the flow separation although the recirculation region is much shorter than the real one as discussed below.

Table I summarizes the results in terms of prediction of the streamwise locations of the separation and the reattachement points. As already mentioned by Temmerman *et al.*[13] and Breuer *et al.*,[14] the ability to correctly reproduce the

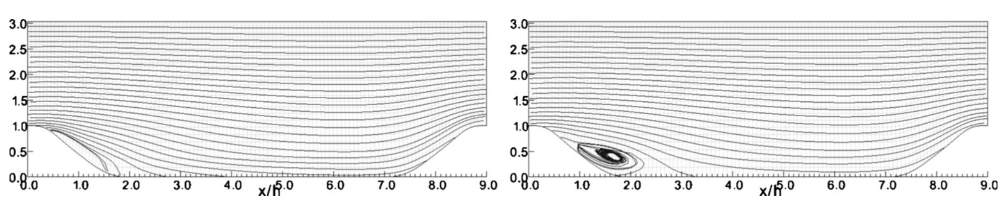

FIG. 15. Mean streamlines obtained with grid B for MPB model (left) and the present model (right).

TABLE I. Streamwise location of the separation, $(x/h)_{sep}$, and the reattachement, $(x/h)_{reat}$, points in the various simulations performed.

Grid	Wall treatment	$(x/h)_{sep}$	$(x/h)_{reat}$	$(x/h)_{reat}-(x/h)_{sep}$
Grid A	No-slip	0.30	5.03	4.73
Grid A	SWM	0.53	2.68	2.15
Grid A	MPB	0.38	4.27	3.89
Grid A	Present model	0.38	4.65	4.27
Grid B	No-slip	0.61	2.82	2.21
Grid B	SWM	⋯	⋯	⋯
Grid B	MPB	0.53	2.97	2.44
Grid B	Present model	0.45	3.92	3.47
Grid C	No-slip	⋯	⋯	⋯
Grid C	SWM	⋯	⋯	⋯
Grid C	MPB	⋯	⋯	⋯
Grid C	Present model	0.68	2.97	2.29
Breuer *et al.*[a]	No-slip	0.190	4.694	4.504
Temmerman *et al.*[b]	No-slip	0.22	4.72	4.5

[a]Reference 14.
[b]Reference 13.

length of the separated region is a good indicator of the model quality. Indeed, the worst the model is, the later the flow separates and the sooner it reattaches. In that respect, SWM model predicts the shorter recirculation bubble with grid A. Conversely, the other three investigated cases yield comparable length not too far from the reference value. For grid B, the SWM model is no-longer able to predict the reverse flow region. The MPB model and the no-model cases both yield a very reduced length for the recirculation bubble and the largest length is predicted by our model. As previously stated, for grid C, only the present model is able to predict a reverse flow region. It is important to remark that the streamwise discretization being very coarse it is therefore difficult to precisely predict the exact flow separation. Indeed, the difference between the location of the separation point predicted by our model and the LES of reference is only six times the streamwise cell size for the grid C case.

V. CONCLUSIONS

A new model is constructed to approximate the velocity profile in the near-wall region of turbulent flows subjected to streamwise pressure gradients. The model is based on the simplified thin-boundary-layer equations and on a turbulent viscosity coefficient whose formulation is an extension of the ones originally proposed by Nituch *et al.*[20] and Balaras *et al.*[2] In particular, the turbulent viscosity involves a damping function which is a function of the intensity of the streamwise pressure gradient. The model validation is first made through *a priori* tests with various flow configurations with and without streamwise pressure gradients and with an eventual flow separation. From the performed comparisons, it is shown that the model is accurate until roughly 100 wall units. The present wall model is then used in LES computations as wall boundary condition with the definition of a corrective viscosity in the first cells at the vicinity of the wall. LESs using the present model are then performed for various flow configurations such as a turbulent channel flow and the flow over a periodic hill arrangement. The model is compared with success to several previous wall models of the literature. It yields good results for first order statistics even when the first grid point away from the wall is located in the logarithmic boundary-layer region. The results clearly demonstrate the importance of taking into account both streamwise pressure gradient effects and Reynolds stresses in the wall modeling. In particular, for flows with adverse pressure gradient, the present model is able to reproduce flow separation even when very coarse grids are considered. It is important to point out that the present wall model can also be applied for RANS simulations and thus widely used for practical applications.

ACKNOWLEDGMENTS

The authors want to thank DFG-CNRS work group for letting their numerical data available. The authors acknowledge Christophe Brun for valuable discussions. The authors gratefully acknowledge funding by ADEME, by Alstom Hydro France, and by ANR through the SIET project.

[1]D. R. Chapman, "Computational aerodynamics development and outlook," AIAA J. **17**, 1293 (1979).
[2]E. Balaras, C. Benocci, and U. Piomelli, "Two-layer approximate boundary conditions for large-eddy simulation," AIAA J. **34**, 1111 (1996).
[3]P. R. Spalart, W. H. Jou, M. Strelets, and S. R. Allmaras, Comments on the feasibility of LES for wings and on a hybrid RANS/LES approach in *Advances in DNS/LES*, edited by C. Lu and Z. Liu (Greyden Press, Columbus, 1997), pp. 137–148.
[4]J. Fröhlich and D. von Terzi, "Hybrid LES/RANS methods for simulation of turbulent flows," Prog. Aerosp. Sci. **44**, 349 (2008).
[5]U. Schumann, "Subgrid-scale model for finite difference simulations of turbulent flows in plane channels and annuli," J. Comput. Phys. **18**, 376 (1975).
[6]G. Grötzbach, *Direct Numerical and Large Eddy Simulation of Turbulent Channel Flows* (2nd ed.), in Encyclopedia of Fluid Mechanics Vol. 6, edited by N. P. Cheremisinoff (Gulf Publ., West Orange, NJ, 1986).
[7]D. B. Spalding, "A single formula for the law of the wall," Trans. ASME, J. Appl. Mech. **28**, 455 (1961).
[8]W. Cabot and P. Moin, "Approximate wall boundary conditions in the large-eddy simulation of high reynolds number flow," Flow, Turbul. Combust. **63**, 269 (2000).
[9]U. Piomelli and E. Balaras, "Wall-layer models for large-eddy simulations," Annu. Rev. Fluid Mech. **34**, 349 (2002).
[10]U. Piomelli, "Wall-layer models for large-eddy simulations," Prog. Aerosp. Sci. **44**, 437 (2008).
[11]M. Manhart, N. Peller, and C. Brun, "Near-wall scaling for turbulent boundary-layers with adverse pressure gradient," Theor. Comput. Fluid Dyn. **22**, 243 (2008).
[12]A. G. Kravchenko, P. Moin, and R. Moser, "Zonal embedded grids for numerical simulations of wall-bounded turbulent flows," J. Comput. Phys. **127**, 412 (1996).
[13]L. Temmerman, M. A. Leschziner, C. P. Mellen, and J. Fröhlich, "Investigation of wall-function approximations and subgrid-scale models in large eddy simulation of separated flow in a channel with streamwise periodic constrictions," Int. J. Heat Fluid Flow **24**, 157 (2003).
[14]M. Breuer, B. Kniazev, and M. Abel, "Development of wall models for LES of separated flows using statistical evaluations," Comput. Fluids **36**, 817 (2007).
[15]M. Wang and P. Moin, "Dynamic wall modeling for large-eddy simulation of complex turbulent flows," Phys. Fluids **14**, 2043 (2002).
[16]R. L. Simpson, "A model for the backflow mean velocity profile," AIAA J. **21**, 142 (1983).
[17]E. R. van Driest, "On turbulent flow near a wall," J. Aeronaut. Sci. **23**, 1007 (1956).
[18]T. Cebeci, "Behavior of turbulent flow near a porous wall with pressure gradient," AIAA J. **8**, 2152 (1970).
[19]B. E. Launder and C. H. Priddin, "A comparison of some proposals for the

mixing length near a wall," Int. J. Heat Mass Transfer **16**, 700 (1973).
[20] M. J. Nituch, S. Sjolander, and M. R. Head, "An improved version of the Cebeci-Smith eddy-viscosity model," Aeronaut. Q. **29**, 207 (1978).
[21] R. D. Moser, J. Kim, and N. N. Mansour, "DNS of turbulent channel flow up to $\mathrm{Re}_\tau=590$," Phys. Fluids **11**, 943 (1999).
[22] C. Fureby, G. Tabor, H. G. Weller, and A. D. Gosman, "A comparative study of subgrid scale models in homogeneous isotropic turbulence," Phys. Fluids **9**, 1416 (1997).
[23] M. H. Baba-Ahmadi and G. Tabor, "Inlet conditions for LES of gas-turbine swirl injectors," AIAA J. **46**, 1782 (2008).
[24] C. Duprat, G. Balarac, O. Métais, and T. Laverne, "Simulation des grandes échelles d'un aspirateur de centrale hydraulique," Mécanique & Industries **10**, 211 (2009).
[25] C. M. Rhie and W. L. Chow, "Numerical study of the turbulent flow past an airfoil with trailing edge separation," AIAA J. **21**, 1525 (1983).
[26] A. Yoshizawa and K. Horiuti, "A statistically-derived subgrid-scale kinetic energy model for the large-eddy simulation of turbulent flows," J. Phys. Soc. Jpn. **54**, 2834 (1985).
[27] S. Ghosal, T. Lund, P. Moin, and K. Akselvoll, "A dynamic localization model for large-eddy simulation of turbulent flows," J. Fluid Mech. **286**, 229 (1995).
[28] S. Jakirlic, R. Jester-Zürker, and C. Tropea, Workshop on Refined Turbulence Modeling. Ninth ERCOFTAC/IAHR/COSTCS, Darmstadt University of Technology, Germany, 4–5 October 2001 (ERCOFTAC, Lausanne, Switzerland, 2001), Vol. 55, pp. 36–43.
[29] J. Fröhlich, C. P. Mellen, W. Rodi, L. Temmerman, and M. Leschziner, "Highly resolved large-eddy simulation of separated flow in a channel with streamwise periodic constrictions," J. Fluid Mech. **526**, 19 (1999).
[30] C. Mellen, J. Fröhlich, and W. Rodi, in "Large-eddy simulation of the flow over periodic hills," edited by M. Deville and R. Owens, Proceedings of the 16th IMACS World Congress, Lausanne, Switzerland, 2000 (unpublished).
[31] A. Keating and U. Piomelli, "A dynamic stochastic forcing method as a wall-layer model for large-eddy simulation," J. Turbul. **7**, 1 (2006).
[32] L. Davidson and M. Billson, "Hybrid LES/RANS using synthesized turbulence for forcing at the interface," Int. J. Heat Fluid Flow **27**, 1028 (2006).
[33] M. Germano, U. Piomelli, P. Moin, and W. H. Cabot, "A dynamic subgrid-scale eddy viscosity model," Phys. Fluids A **3**, 1760 (1991).